Ultra-Wide Voltage Range Reconfigurable DAB Converter for Universal PEV Charging Stations

Yingjian Zhuge[1], Linyan Lu[1], Dongdong Shu[1], Haoyu Wang[*1,2]
[1] *School of Information Science and Technology, ShanghaiTech University, Shanghai, China*
[2] *Shanghai Engineering Research Center of Energy Efficient and Custom AI IC, Shanghai, China*
[*] Corresponding Author: wanghy@shanghaitech.edu.cn

2025 IEEE Energy Conversion Congress & Exposition Asia (ECCE-Asia) | 979-8-3315-1886-8/25/$31.00 ©2025 IEEE | DOI: 10.1109/ECCE-Asia63110.2025.11112374

***Abstract*—In universal plug-in electric vehicle (PEV) charging applications, dual-active-bridge(DAB) converters must operate across an ultra-wide voltage range. However, their performance deteriorates significantly under large output voltage variations. To address this challenge, we propose a reconfigurable DAB converter utilizing a four-winding transformer. This design enables three distinct transformer turns ratios, dividing the total output voltage range into three segments, each operating within a substantially narrower gain range. A simple single-phase shift modulation method is employed to achieve high efficiency within each targeted gain segment. A 330 W prototype was developed to validate the concept. Experimental results demonstrate consistent efficiency across an ultra-wide output voltage range of 70 V to 260 V, with a peak efficiency of 97.07%.**

***Index Terms*—Plug-in electric vehicle (PEV), dual-active-bridge (DAB), wide voltage gain range, universal charging.**

I. Introduction

The development of ultra-fast charging (UFC) systems has emerged as a critical enabler for the electrification of transportation, overcoming key challenges in energy replenishment and compatibility with varying battery voltage levels, as detailed in Table I. The ultra-wide output voltage range (typically 200–1000 V) and dynamic load demands imposed by these systems present significant design challenges, especially for the rear-stage DC/DC converter within charging systems [1]–[3]. Modern research efforts increasingly prioritize bidirectional power flow functionality, which strengthens grid resilience by enabling dynamic load management and facilitating the integration of distributed energy resources [4], [5]. Among emerging solutions, Dual Active Bridge (DAB) converters have gained prominence due to their galvanic isolation, inherent bidirectional power transfer capability, wide operational voltage range, and high-power-density design.

When the input and output voltages of the DAB converter are mismatched (i.e., $M \neq 1$), zero voltage switching (ZVS) may be compromised, resulting in significant backflow power and elevated current stress. Various advanced modulation strategies with additional control variables have been proposed to address the limitations of traditional Single-Phase-Shift (SPS) modulation, which provides only one degree of control. These include Extended-Phase-Shift (EPS) control [6], [7], Dual-Phase-Shift (DPS) control [8], and Triple-Phase-Shift (TPS) control [9], [10].

This work was supported in part by the National Natural Science Foundation of China under Grant 52077140.

For instance, the modulation technique presented in [11] employs an adaptive duty cycle combined with phase shift modulation to ensure full ZVS across a universal input voltage range. Likewise, [12] introduces an asymmetric half-frequency modulation approach to optimize the operation of DAB converters near unity voltage gain. Furthermore, frequency modulation has been demonstrated to significantly improve performance under light-load conditions [13]. However, the incorporation of additional degrees of freedom and operation modes inherently escalates the complexity of both the circuit and control strategy.

Another promising approach is topology reconstruction. In [14], an alternative-fed DAB converter is introduced, combining the strengths of both voltage-fed and current-fed architectures while mitigating their respective drawbacks. Two-stage circuit configurations have also demonstrated effectiveness, with non-isolated DC/DC circuits handling voltage regulation. This allows the DAB converter to operate under voltage-matching conditions, significantly improving performance. For instance, the cascade configuration of a DAB converter with a buck-boost converter, as presented in [15], achieves exceptional performances across a wide input voltage range. However, since the front-end converter processes the entire system power, it incurs notable losses. In [16], the quasi-two-stage buck-DAB converter addresses this issue by routing only a portion of the transmitted power through the front-end circuit, thereby reducing losses in the buck stage. Meanwhile, [17] explores the two-stage circuits with parallel inputs, albeit at the cost of isolation. Additionally, by integrating a transformer and connecting it with one bridge arm and the intermediate point of the input capacitor bridge, this structure can provide $\pm V_{in}$ and $\pm V_{in}/2$ voltage levels, further enhancing operational performance [18]. However, the gain range of this design remains limited.

In this paper, we propose an ultra-wide gain range bidirectional charger featuring a reconfigurable transformer. The remainder of the paper is structured as follows: Section II introduces the fundamental operating modes of the proposed converter. Section III delves into the detailed design considerations for the transformer and inductor, accompanied by an analysis of the ZVS range. Following this, Section IV presents the implementation of a prototype for the reconfigurable DAB converter to validate the proposed topology. Finally, Section V concludes the paper.

Authorized licensed use limited to: ShanghaiTech University. Downloaded on July 28,2026 at 12:56:14 UTC from IEEE Xplore. Restrictions apply.

TABLE I: Technical Specifications of state-of-the-art dc ultra-fast chargers

Manufacturer	INFY POWER	Winline Technology	KSTAR	Sinexcel	Sungrow	Tesla
Model	IDS800K1K-LWR	YLCES720KL	/	SEV1000/800F-7	IDC640	SUPERCHARGER V4
Rated Power	800kW	720kW	720kW	800kW	640kW	600 kW
Module Configuration	40kW×20	/	/	40kW×20	40kW×16	/
Intput Voltage	380V±15%	380V±15%	380V±20%	380V±15%	380V±15%	380V–480V (-5%, +10%)
Output Voltage	150V-1000V	200-1000Vdc	200-1000V	200V-1000V	200V-1000V	400-1000V
Rated Charging Current	600A	600A	600A	600A	600A	615A
Cooling	Liquid Cooling	Liquid Cooling	Liquid Cooling	Liquid Cooling	Liquid Cooling	Liquid Cooling
Peak Efficiency	>95.5%	>95%	≥95%	>96.3%	≥96.5%	>96%
Volume	3960L	2924L	1872L	2705.4L	2732.4L	/

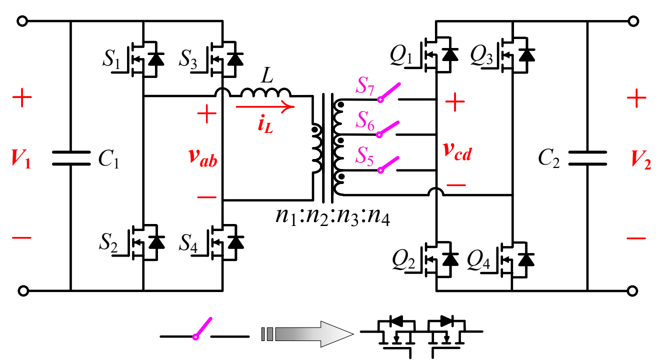

Fig. 1: Schematic of proposed DAB converter based on an adjustable turns ratio transformer.

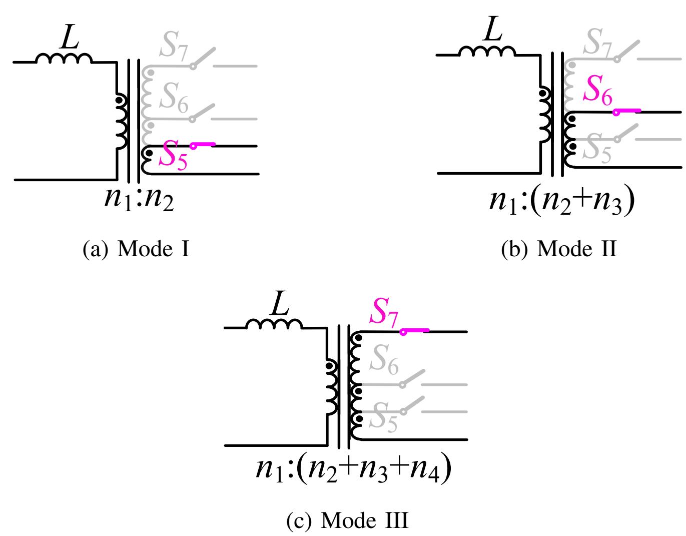

(a) Mode I

(b) Mode II

(c) Mode III

Fig. 2: Three operation modes of the proposed reconfigurable DAB converter.

II. Topology Description

The proposed DAB converter, as shown in Fig. 1, comprises primary and secondary full bridges, an inductor, an isolated transformer, and three four-quadrant switches S_{5-7}. The transformer features a four-winding structure with turns n_{1-4}. The secondary side can select the winding connected to the circuit through the four-quadrant switches to be n_2, $n_2 + n_3$, or $n_2 + n_3 + n_4$.

Based on the three transformer structures, the proposed converter exhibits three operation modes accordingly, as shown in Fig. 2. Since the entire gain range is divided into three segments, the gain range that each segment needs to handle is significantly narrowed, allowing a simple SPS modulation to achieve a good performance. The constant voltage (CV) operation point that requires prolonged operation can be designed at M = 1 for optimal performance. Additionally, due to the high voltage utilization rate, the maximum transmission power capability of the converter can be more fully utilized.

III. Design Considerations

Regarding the design of the proposed DAB converter, the following key steps are undertaken.

A. Transformer Design

Since the proposed converter has three turn ratios, selecting the appropriate turns ratio in different gain ranges can effectively improve the performance. The turns ratio n of different modes is n_2/n_1, $(n_2+n_3)/n_1$, or $(n_2+n_3+n_4)/n_1$, respectively.

$$\begin{aligned} &\text{Mode I} : \mathrm{n} = \mathrm{n_2}/\mathrm{n_1} \\ &\text{Mode II} : \mathrm{n} = (\mathrm{n_2}+\mathrm{n_3})/\mathrm{n_1} \\ &\text{Mode III} : \mathrm{n} = (\mathrm{n_2}+\mathrm{n_3}+\mathrm{n_4})/\mathrm{n_1} \end{aligned} \tag{1}$$

To achieve better performance, the CV operation point during the charging process can be designed at $M = 1$ with optimal performance. Therefore, the turns ratios should meet the following equations:

$$\frac{n_2+n_3}{n_1} = \frac{V_{CV1}}{V_1} \tag{2}$$

$$\frac{n_2+n_3+n_4}{n_1} = \frac{V_{CV2}}{V_1} \tag{3}$$

The turns ratio required by Mode I is lower than that of Mode II, and the operation performance of the lowest voltage

Authorized licensed use limited to: ShanghaiTech University. Downloaded on July 28,2026 at 12:56:14 UTC from IEEE Xplore. Restrictions apply.

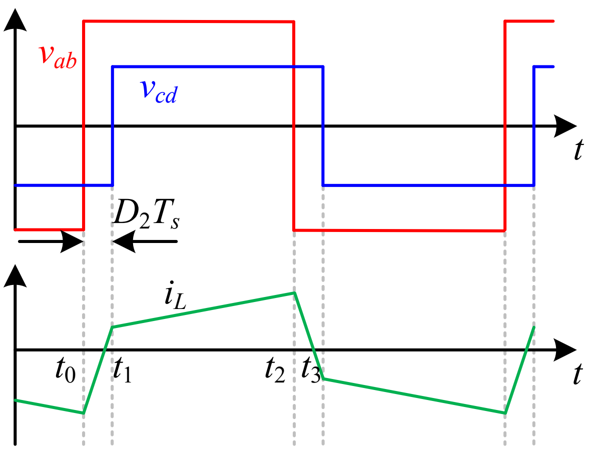

(a) Critical steady-state waveforms.

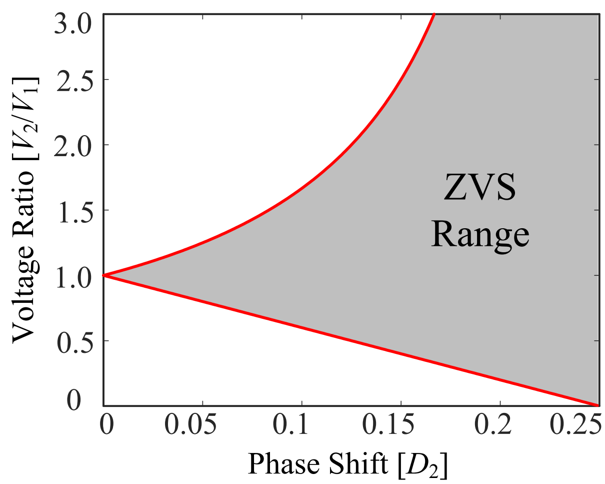

(b) ZVS range.

Fig. 3: ZVS region and key waveforms under SPS modulation.

should be guaranteed. Therefore, the range of turns ratio of Mode I is:

$$\frac{V_{CV1}}{V_1} > \frac{n_2}{n_1} > \frac{V_{CC,min}}{V_1} \tag{4}$$

B. ZVS Range Analysis

Since the three turns ratios of the proposed converter partition the gain range into three distinct segments, the gain range within each segment is significantly narrowed. As a result, SPS modulation can achieve excellent performance. The voltage and current waveforms under SPS modulation are illustrated in Fig. 3(a). Notably, the currents at t_0 and t_1 are symmetric with respect to those at t_2 and t_3 along the horizontal axis. Leveraging these waveform characteristics, the expressions for the currents at t_0 and t_1 can be derived as follows:

$$\begin{cases} i_L(t_0) = \frac{V_2T_s}{4nL} - \frac{V_1T_s}{4L} - \frac{V_2D_2T_s}{nL} \\ i_L(t_1) = \frac{V_2T_s}{4nL} - \frac{V_1T_s}{4L} + \frac{V_1D_2T_s}{L} \end{cases} \tag{5}$$

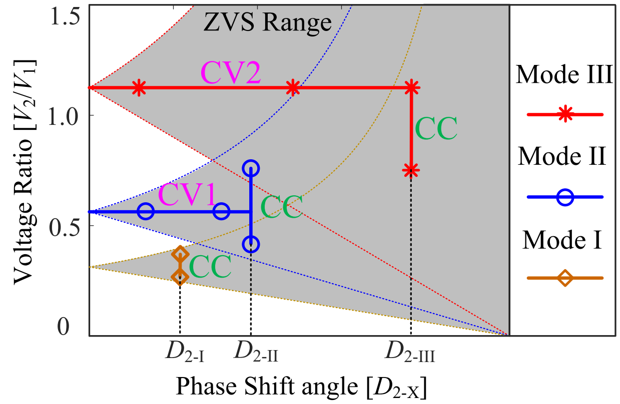

Fig. 4: ZVS region of the proposed DAB converter based on four windings transformer.

To achieve soft-switching operation in this converter, the inductor current at t_0 must be negative, while at t_1, it must be positive. Consequently, the ZVS range can be derived as a function of the voltage ratio M, given by:

$$1 - 4D_2 < M < \frac{1}{1 - 4D_2} \tag{6}$$

The ZVS range of the converter under various voltage ratios, when the transformer turns ratio is $n = 1$, is depicted in Fig. 3(b). As illustrated in the figure, when M deviates from 1, the converter is more likely to lose ZVS under light-load conditions, particularly with a small phase shift angle. Conversely, under heavy-load conditions with a larger phase shift angle, the ZVS range is significantly extended. Additionally, when $M = 1$, the converter achieves ZVS across a wide load range, making it particularly well-suited for CV operation with a fixed voltage ratio.

The ZVS region of the proposed DAB converter is shown in Fig. 4. Two CV operation points are intentionally designed at the $M = 1$ point of Mode II and Mode III. For a converter with fixed parameters, the output current in each mode depends solely on the phase shift angle D_2. Let D_{2-X}(where X = I, II, III) denote the phase shift angle in each mode during the constant current (CC) charging process, which remains constant within each mode. Furthermore, the three turns ratios significantly expand the ZVS region, enabling the converter to be optimally designed to ensure ZVS throughout the charging process.

C. Inductor Design

The DAB converters realize power transmission by controlling the inductor current, so it is necessary to design the inductor reasonably. The design process of the inductor is carried out at the peak power point. The phase shift angle D_2 and I_{peak} satisfy the following relationships:

$$D_2 = \frac{1 - \sqrt{1 - \frac{8nf_sPL}{V_1V_2}}}{4} \tag{7}$$

$$I_{peak} = \frac{T_sV_1}{4L}[1 - \sqrt{1 - \frac{8nf_sPL}{V_1V_2}}] \tag{8}$$

Authorized licensed use limited to: ShanghaiTech University. Downloaded on July 28,2026 at 12:56:14 UTC from IEEE Xplore. Restrictions apply.

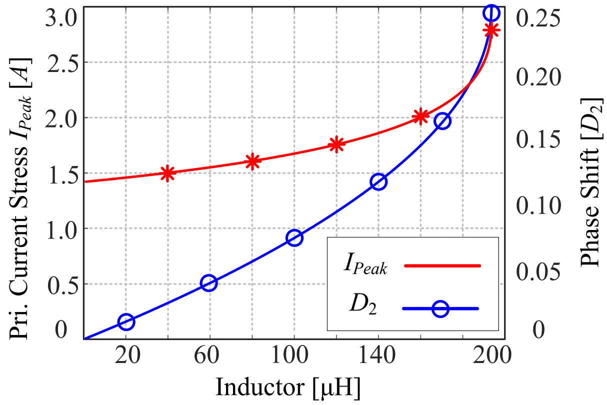

Fig. 5: D_2 and I_{peak} versus inductance value at peak power.

Fig. 5 illustrates the relationships between the primary side current stress I_{peak}, phase shift angle D_2, and inductance L, with an input voltage of 220V, an output voltage of 260V, and a power level of 330W at a frequency of 100kHz. A smaller inductance corresponds to a smaller phase shift angle, reducing the current stress. However, this comes with a limited ZVS range. When D_2 approaches the maximum phase shift angle of 0.25, the current stress increases rapidly with the rise in inductance L. Therefore, positioning the peak power slightly below the maximum power transfer capability can enhance the operation performance.

Fig. 6 illustrates the relationship between the primary and secondary current stresses of the proposed converter and the battery voltage across its operational range. For comparison, a conventional DAB converter with a voltage matching point designed at $V_2 = 170$V and an equivalent phase shift angle is included.

As shown in Fig. 6(a), the primary-side current stress of the proposed topology remains lower over a wide voltage range, except for a slightly higher stress near the voltage matching region of the conventional topology. This occurs because the CV charging gain points in the proposed design are intentionally aligned with the voltage matching condition to enhance overall performance, resulting in elevated current stress during the intermediate transition phase between Mode II and Mode III compared to the conventional optimal region. During CV operation, when the battery voltage reaches 260V, the conventional DAB loses ZVS capability on the primary side if the phase shift angle falls below 0.0865, corresponding to a 60% full-load condition.

Fig. 6(b) depicts the secondary-side current stress versus battery voltage. Similarly, the proposed topology exhibits marginally higher stress only within the voltage matching region of the conventional counterpart. In CV mode, the conventional DAB fails to maintain ZVS on the secondary side at a battery voltage of 130V when the phase shift angle is below 0.0588, equivalent to a 44% full-load condition.

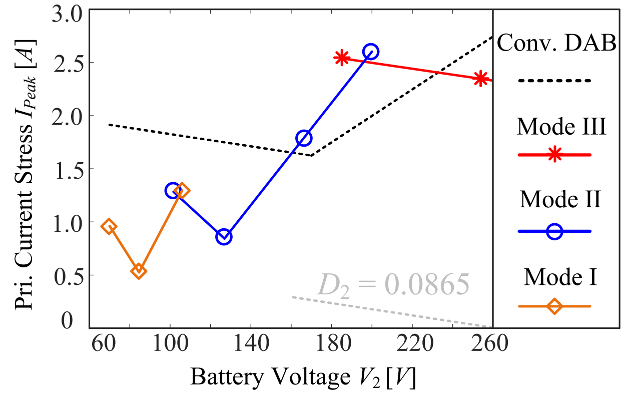

(a) Primary side current stress

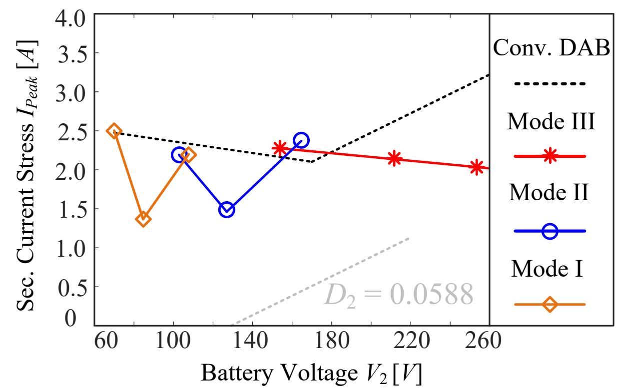

(b) Secondary side current stress

Fig. 6: Current stresses of the primary and secondary sides.

IV. Experimental Results

The experimental analysis verifies the operation of the designed system under distinct operating conditions. A proof-of-concept laboratory prototype is developed to verify the performance of the designed OBC. The selection of parameters for the prototype is carried out according to the design criteria discussed in Section III, as depicted in Table II. A DSP controller (TMS320F28335) from Texas Instruments is employed to realize the control algorithms.

The steady-state waveforms of the designed prototype are captured in Fig. 7 with constant V_1 and different V_2=130V, 260V, respectively. Since the operating state is designed at the input and output voltage matching points of Mode II and Mode III, the converter has a lower current stress. It can be observed that the MOSFETs drain-source voltages drop to zero before the gate signal is applied. Therefore, the ZVS of all MOSFETs is well realized in all scenarios.

Fig. 8 illustrates the efficiency of the designed prototype across its various operating modes. The results demonstrate that the converter achieves relatively high efficiency near the input-output voltage matching points in each mode. However, when the input-output voltage ratio deviates from unity, the efficiency experiences a decline. The three transformer ratios incorporated into the converter ensure optimal performance across the entire operating range, achieving a peak efficiency of up to 97.07% and maintaining an overall efficiency exceeding 94.5%.

Authorized licensed use limited to: ShanghaiTech University. Downloaded on July 28,2026 at 12:56:14 UTC from IEEE Xplore. Restrictions apply.

TABLE II: Design Parameters

Symbol	Parameters	Value	Symbol	Parameters	Value
V_1	Bus voltage	220V	$n_1 : n_2 : n_3 : n_4$	turn ratio	22:8:5:13
V_2	battery voltage	70-260V	L	Primary side inductor	$180\mu H$
f_s	switching frequency	100kHz	D_{2-I}	Mode I phase shift	0.043
t_d	dead time	200ns	D_{2-II}	Mode II phase shift	0.069
I_{CC}	constant current	1.3A	D_{2-III}	Mode III phase shift	0.192

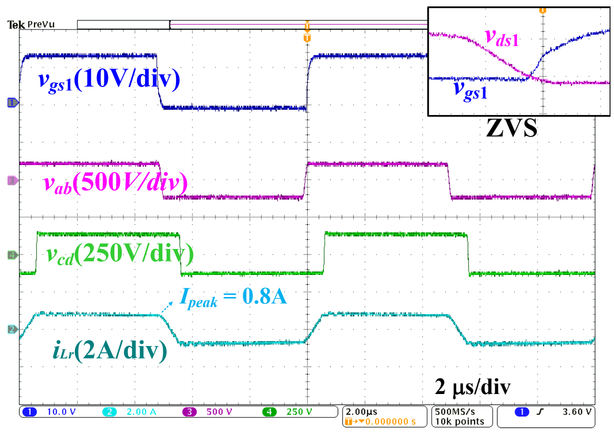

(a) V_2=130V

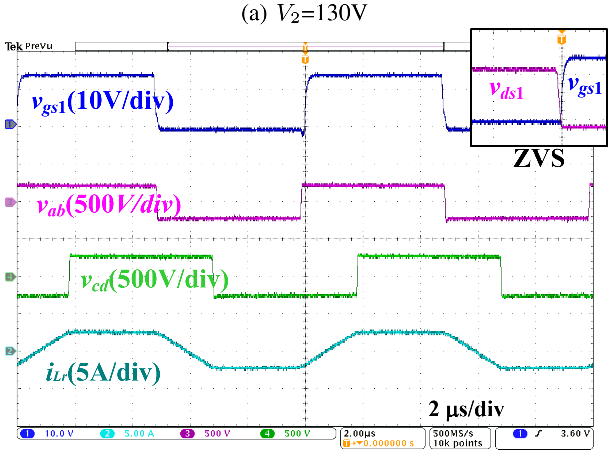

(b) V_2=260V

Fig. 7: Key experimental waveforms when V_2 is 130V and 260V.

V. Conclusions

In this paper, an ultra-wide gain bidirectional PEV charger solution employing a four-winding transformer is proposed. Based on a reconfigurable DAB topology, the proposed scheme achieves three distinct effective transformer ratios by controlling the four-winding transformer using three switches. This approach allows the converter to operate in three different modes, significantly expanding its gain range. In each operational mode, the converter functions within an optimized range, ensuring that the input and output voltages remain well-matched. This reduces the current stress on both the primary and secondary sides of the converter, thereby enhancing the performance of the switches. The adoption of a relatively simple single-phase-shift modulation technique further improves operational efficiency and power utilization. Experimental verification is conducted on a 330W laboratory prototype, which achieves a peak efficiency of 97.07% and an overall efficiency exceeding 94.5%.

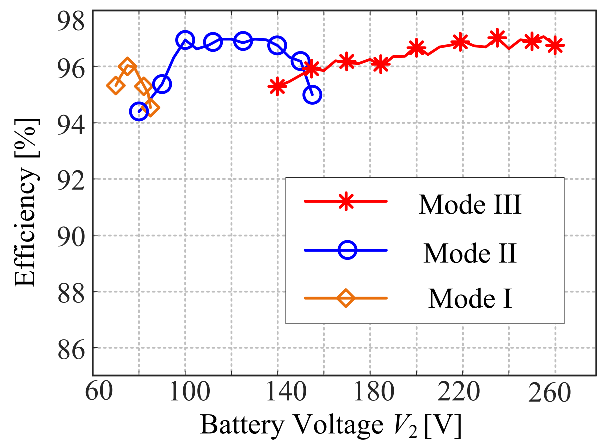

Fig. 8: Measured efficiency.

References

[1] C. Li, M. Zhou, and H. Wang, "An H5-Bridge-Based Asymmetric LLC Resonant Converter With an Ultrawide Output Voltage Range," *IEEE Trans. Ind. Electron.*, vol. 67, no. 11, pp. 9503–9514, Nov. 2020.

[2] D. Shu and H. Wang, "An Ultrawide Output Range LLC Resonant Converter Based on Adjustable Turns Ratio Transformer and Reconfigurable Bridge," *IEEE Trans. Ind. Electron.*, vol. 68, no. 8, pp. 7115–7124, Aug. 2021.

[3] M. Zhou, D. Shu, and H. Wang, "An H5-Bridge-Based Laddered CLLC DCX With Variable DC Link for PEV Charging Applications," *IEEE Trans. Power Electron.*, vol. 37, no. 4, pp. 4249–4260, Apr. 2022.

[4] U. Khalid, D. Shu, and H. Wang, "Hybrid Modulated Reconfigurable Bidirectional CLLC Converter for V2G Enabled PEV Charging Applications," in *Proc. IEEE Appl. Power Electron. Conf. Expo. (APEC),* Anaheim, CA, Mar. 2019, pp. 3332–3338.

[5] H. Wouters and W. Martinez, "Bidirectional onboard chargers for electric vehicles: State-of-the-art and future trends," *IEEE Trans. Power Electron.*, vol. 39, no. 1, pp. 693–716, Jan. 2024.

[6] H. Shi *et al.*, "Minimum-Backflow-Power Scheme of DAB-Based Solid-State Transformer With Extended-Phase-Shift Control," *IEEE Trans. Ind. Appl.*, vol. 54, no. 4, pp. 3483–3496, Jul. 2018.

[7] J. Tian, F. Wang, F. Zhuo, Y. Wang, H. Wang, and Y. Li, "A Zero-Backflow-Power EPS Control Scheme With Multiobjective Coupled-Relationship Optimization in DAB-Based Converter," *IEEE J. Emerging Sel. Top. Power Electron.*, vol. 10, no. 4, pp. 4128–4145, Aug. 2022.

[8] S. Chaurasiya and B. Singh, "A Load Adaptive Hybrid DPS Control for DAB to Secure Minimum Current Stress and Full ZVS Operation Over Wide Load and Voltage Conversion Ratio," *IEEE Trans. Ind. Appl.*, vol. 59, no. 2, pp. 1901–1911, Mar. 2023.

Authorized licensed use limited to: ShanghaiTech University. Downloaded on July 28,2026 at 12:56:14 UTC from IEEE Xplore. Restrictions apply.

[9] S. Shao, M. Jiang, W. Ye, Y. Li, J. Zhang, and K. Sheng, "Optimal Phase-Shift Control to Minimize Reactive Power for a Dual Active Bridge DC–DC Converter," *IEEE Trans. Power Electron.*, vol. 34, no. 10, pp. 10 193–10 205, Oct. 2019.
[10] F. Lin, X. Zhang, X. Li, C. Sun, W. Cai, and Z. Zhang, "Automatic Triple Phase-Shift Modulation for DAB Converter With Minimized Power Loss," *IEEE Trans. Ind. Appl.*, vol. 58, no. 3, pp. 3840–3851, May 2022.
[11] H. Kim, J. Park, J. Lee, and S. Choi, "A simple modulation strategy for full zvs of single-stage electrolytic capacitor-less ev charger with universal input," *IEEE Trans. Power Electron.*, vol. 37, no. 10, pp. 12 030–12 040, Oct. 2022.
[12] A. Kazemtarghi, S. Dey, A. Mallik, and N. G. Johnson, "Asymmetric Half-Frequency Modulation in DAB to Optimize the Conduction and Switching Losses in EV Charging Applications," *IEEE Trans. Transp. Electrif.*, vol. 9, no. 3, pp. 4196–4210, Sep. 2023.
[13] Z. Xiao, M. Xiao, Z. He, L. Wang, Z. Li, and H. Wang, "Light load efficiency improvement of dab converters with optimal switching sequences," *IEEE Trans. Power Electron.*, pp. 1–14, 2024.
[14] Y. Zhang, N. Hou, and Y. Li, "An alternative-fed dual-active-bridge dc/dc converter with wide voltage gains and low current ripples," *IEEE Trans. Power Electron.*, vol. 39, no. 7, pp. 7823–7827, Jul. 2024.
[15] C. Xu *et al.*, "A Novel Converter Integrating Buck-Boost and DAB Converter for Wide Input Voltage," in *Proc. IEEE Ann. Conf. IEEE Ind. Electron. Soc. (IECON),* Singapore, Oct. 2020, pp. 2877–2882.
[16] Z. Lu, G. Xu, W. Xiong, Y. Sun, and M. Su, "A quasi-two-stage isolated bidirectional buck-dab converter for wide input voltage range," *IEEE Trans. Power Electron.*, vol. 38, no. 2, pp. 1384–1390, Feb. 2023.
[17] N. Lin, Z. Zhao, F. Diao, Y. Zhao, and J. C. Balda, "A Current-Fed Dual-Half-Bridge-Based Composite Converter With Improved Light-Load Efficiency Through a Multi-Variable Optimization," *IEEE Trans. Transp. Electrif.*, vol. 8, no. 2, pp. 3008–3020, Jun. 2022.
[18] G. Xu, D. Sha, Y. Xu, and X. Liao, "Hybrid-Bridge-Based DAB Converter With Voltage Match Control for Wide Voltage Conversion Gain Application," *IEEE Trans. Power Electron.*, vol. 33, no. 2, pp. 1378–1388, Feb. 2018.

Authorized licensed use limited to: ShanghaiTech University. Downloaded on July 28,2026 at 12:56:14 UTC from IEEE Xplore. Restrictions apply.